ChemPubSoc Europe

DOI: 10.1002/cssc.201600940

CHEMSUSCHEM Full Papers

Electron Transport Layer-Free Solar Cells Based on Perovskite–Fullerene Blend Films with Enhanced Performance and Stability

Jorge Pascual,[a, b] Ivet Kosta,[a] T. Tuyen Ngo,[c] Andrey Chuvilin,[d, f] German Cabanero,[a] Hans J. Grande,[a] Eva M. Barea,[c] Iván Mora-Seró,*[c] Juan Luis Delgado,*[b, e, f] and Ramon Tena-Zaera*[a]

Dedicated to Prof. Jean-François Nierengarten on the occasion of his 50th birthday

The solution processing of pinhole-free methylammonium lead triiodide perovskite–C_{70} fullerene ($MAPbI_3$:C_{70}) blend films on fluorine-doped tin oxide (FTO)-coated glass substrates is presented. Based on this approach, a simplified and robust protocol for the preparation of efficient electron-transport layer (ETL)-free perovskite solar cells is described. Power conversion efficiency (PCE) of 13.6% under AM 1.5 G simulated sunlight is demonstrated for these devices. Comparative impedance spectroscopy and photostability analysis of the $MAPbI_3$:C_{70} and single $MAPbI_3$ films compared with conventional compact TiO_2 ETL-based devices are shown. The beneficial impact of using $MAPbI_3$:C_{70} blend films is emphasized.

Introduction

Since the pioneering work on full solid-state halide perovskite solar cells,[1,2] solution-processed perovskite films became key players in photovoltaics (PV) owing to their unique combination of versatile processing and optoelectronic properties.[3] However, further progress on the solar cell architecture and complementary materials (e.g., charge-selective contacts) is still needed to realize the potential of these devices. As an example, in regular architecture perovskite solar cells, with the general structure: glass/electron-transport layer (ETL)/absorber/hole-transport layer (HTL)/back contact, the deposition of the usual TiO_2 ETL results in significant limitations for the substrate choice owing to high processing temperatures (i.e., generally $\geq$400 °C). This step may indeed be one of the highest energy-demanding processes in perovskite PV manufacturing with a large corresponding impact on the manufacturing cost and energy payback time. Some low-temperature-processed alternative ETLs (e.g., ZnO,[4] SnO_2,[5] and fullerene films[6–8]) have been recently demonstrated. However, their deposition requires an additional step, including additional solvents[4,6,7] and/or techniques,[4,5,8] in the device fabrication. The elimination of the need for a specific ETL in efficient perovskite solar cells remains a challenge, although there are few reports on devices in this area.[9,10] In this context, the recently reported fullerene saturation approach (FSA), which was initially proposed to avoid damage of fullerene ETLs during perovskite processing,[7] opens wide possibilities to process perovskite–fullerene blend films. Indeed, perovskite–phenyl-C_{61}-butyric acid methyl ester (PCBM) blend films have been recently shown as a straightforward approach to improve the fill factor (FF) and suppress hysteresis in perovskite solar cells.[11,12] Furthermore, photostability improvement was also recently reported for devices based on perovskite–PCBM films.[13] Nevertheless, to the best of our knowledge, there are no reports on the use of perovskite–fullerene blend films in semiconducting ETL-free solar cells.

In this paper, the deposition of pinhole-free methylammonium lead triiodide perovskite ($MAPbI_3$)–C_{70} fullerene blend films ($MAPbI_3$:C_{70}) on fluorine-doped tin oxide (FTO)-coated glass

[a] J. Pascual, Dr. I. Kosta, G. Cabanero, Dr. H. J. Grande, Dr. R. Tena-Zaera
Materials Division, IK4-CIDETEC
Parque Tecnológico de San Sebastián
Paseo Miramón, 196, Donostia–San Sebastián 20009 (Spain)
E-mail: rtena@cidetec.es

[b] J. Pascual, Prof. J. L. Delgado
POLYMAT, University of the Basque Country UPV/EHU
Avenida de Tolosa 72 20018 Donostia–San Sebastián (Spain)
E-mail: juanluis.delgado@polymat.eu

[c] T. Tuyen Ngo, Dr. E. M. Barea, Dr. I. Mora-Seró
Institute of Advanced Materials (INAM)
University of Jaume I
Av. de Vicent Sos Baynat, s/n 12006, Castelló de la Plana (Spain)
E-mail: sero@fca.uji.es

[d] Prof. A. Chuvilin
CIC nanoGUNE Consolider
20018 Donostia–San Sebastián (Spain)

[e] Prof. J. L. Delgado
Faculty of Chemistry, University of the Basque Country UPV/EHU
P. Manuel Lardizabal 3, 20018 Donostia–San Sebastián (Spain)

[f] Prof. A. Chuvilin, Prof. J. L. Delgado
Ikerbasque, Basque Foundation for Science
48013 Bilbao (Spain)

Supporting Information and the ORCID identification number(s) for the author(s) of this article can be found under http://dx.doi.org/10.1002/cssc.201600940.

This publication is part of a Special Issue focusing on the "Stability of Perovskite Solar Cells & Devices". A link to the issue's Table of Contents will appear here once it is complete.

substrates is presented, showing the use of the $MAPbI_3$:C_{70} in efficient semiconducting ETL-free perovskite solar cells with commonly used 2,2′,7,7′-tetrakis-(*N*,*N*-di-4-methoxyphenylamino)-9,9′-spirobifluorene (spiro-OMeTAD) as the HTL. In addition, a comparative impedance spectroscopy analysis of the resulting devices (i.e., glass/FTO/$MAPbI_3$:C_{70}/spiro-OMeTAD/Au) compared with analogous devices containing a single perovskite film (i.e., glass/FTO/$MAPbI_3$/spiro-OMeTAD/Au) and a compact TiO_2 (c-TiO_2) ETL (i.e., glass/FTO/c-TiO_2/$MAPbI_3$/spiro-OMeTAD/Au) is also provided. Finally, the photostability of unencapsulated solar cells with the three different architectures is discussed.

Results and Discussion

Perovskite–fullerene blend films

$PbCl_2$, MAI, and C_{70}-containing *N*,*N*—dimethylformamide (DMF)-based formulations (see details in Experimental Section) were used to deposit films on glass/FTO substrates. Figure 1 a shows representative top-view field-emission scanning electron microscopy (FE-SEM) micrographs of the obtained samples. The morphology of the films processed from C_{70}-free solutions on FTO and FTO/c-TiO_2 substrates are also shown (Figure 1 b and 1 c, respectively) for comparison. The mean thickness was in the 400–500 nm range for all films (Figure S1 in the Supporting Information). Interestingly, in contrast to the samples processed from the C_{70}-free solutions that showed significant concentration of pinholes when deposited on the glass/FTO (i.e., bright regions in Figure 1 b), no pinholes were detected in the films processed from C_{70}-containing solutions (Figure 1 a). The latter films showed indeed competitive homogeneity and grain size to the films deposited on the most frequently used glass/c-TiO_2 substrates (Figure 1 c). Therefore, using C_{70}-containing processing solutions appears to be a straightforward approach to improve the pinhole issue in perovskite films directly processed on FTO surfaces, which has been identified as the main limitation of the semiconducting ETL-free perovskite solar cells.[14] The simplicity of C_{70}-containing formulation-based film processing compared with previously proposed approaches, such as FTO ultraviolet/ozone treatment, is a major advantage.[10,15]

The chemical composition of the films processed from C_{70}-containing solutions was investigated by scanning transmission electron microscopy (STEM). Figure 2 displays the high-angle annular dark-field (HAADF) STEM micrographs and chemical maps obtained by electron energy loss spectroscopy (EELS) of carbon K and iodine M edges. At a scale of tens of nm, the carbon distribution (Figure 2 b), determined mainly by the distribution of C_{70} in the film, does not follow the distribution of iodine (Figure 2 c). As is evident from the carbon map, the excess concentration of carbon is observed in linear and circular shapes, which leads to the assumption that C_{70} and/or its derivatives are distributed along the interfaces of the

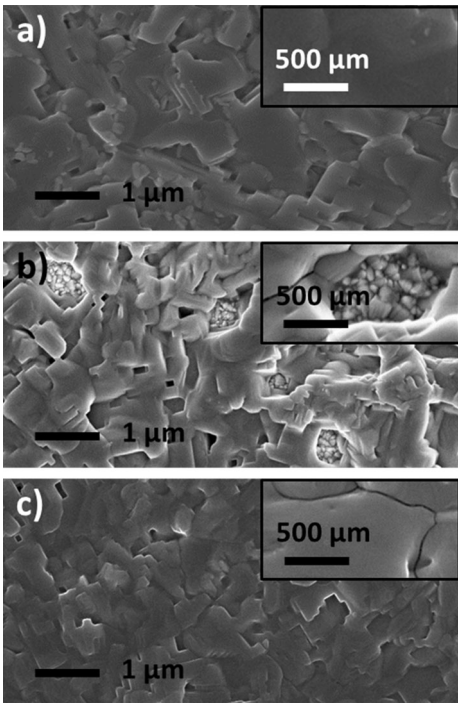

Figure 1. Top-view FE-SEM micrographs of: a) $MAPbI_3$:C_{70} and b) $MAPbI_3$ films deposited on glass/FTO substrates. c) The micrographs of $MAPbI_3$ films deposited on glass/FTO/c-TiO_2. The insets show higher magnification views of a pinhole (b) and grains (a, c).

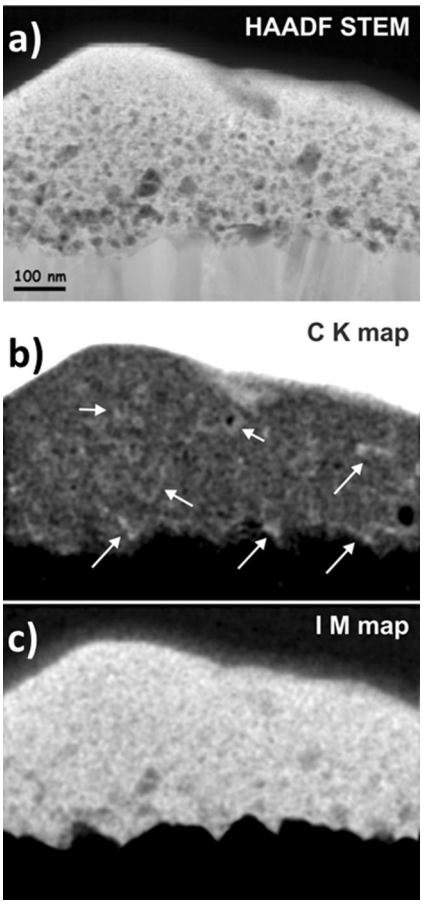

Figure 2. a) HAADF STEM micrograph of the cross section of a glass/FTO/$MAPbI_3$:C_{70} sample and EELS chemical maps of b) carbon K edge and c) iodine M edge. Arrows point to the regions enriched by carbon.

$MAPbI_3$ crystals. Therefore, the inclusion of C_{70} and/or derivatives into the perovskite film was successful. It is noted that the perovskite matrix is referred as $MAPbI_3$ for simplicity; however, deviations from this stoichiometry owing to the preparation of the film from the $PbCl_2$ and MAI precursors cannot be fully ruled out.

Solar cells

The three different types of samples (i.e., glass/FTO/$MAPbI_3$:C_{70}, glass/FTO/$MAPbI_3$ and glass/FTO/c-TiO_2/$MAPbI_3$) were used to prepare solar cells with spiro-OMeTAD and Au as hole-selective and back contact, respectively. As a result, a preliminary series of hybrid halide perovskite solar cells with three different architectures (I, II, and III in Scheme 1) were investigated. Table 1 summarizes the photovoltaic parameters extracted from the *J–V* curves of the best devices (Figure S2).

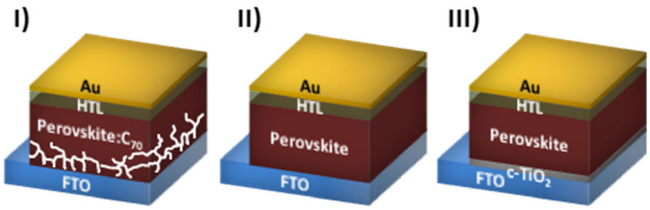

Scheme 1. Three different architectures for perovskite solar cells: devices based on semiconducting ETL-free perovskite (I) and perovskite:C_{70} blend (II) films, and containing a c-TiO_2 ETL (III).

Table 1. Photovoltaic parameters of the best devices from the preliminary series of solar cells with the different architectures (i.e., I, II, and III) under AM 1.5 G simulated sunlight.[a]

Architecture	ETL	J_{SC} [mA cm^{-2}]	V_{OC} [mV]	FF [%]	PCE [%]
I	ETL-free	15.4	1036	73	11.7
II	ETL-free	14.9	1022	70	10.6
III	c-TiO_2	13.4	1014	75	10.2
III	C_{70}[7]	10.9	966	58	6.1
III	C_{70} discont.[7]	15.1	995	69	10.4

[a] The statistical analysis of the photovoltaic parameters, including devices prepared in further series, can be found in Figure S3. Data from solar cells with architecture type III based on the C_{70} ETL (instead of c-TiO_2) are also shown.[7]

Interestingly, a significant increase of the short-circuit current density (J_{SC}) was detected in ETL-free devices (I and II). However, the ETL-based device (III) showed the highest FF value (i.e., 75%), which decreased for devices without ETL. However, devices based on the $MAPbI_3$:C_{70} blend exhibited only a moderate decrease in FF, reaching values close to those based on type III c-TiO_2 (i.e., 73.0%). All in all, an overall improvement in the PV performance, reaching PCE of 11.7%, was detected for the $MAPbI_3$:C_{70} blend-based solar cells. Furthermore, type I devices provided significantly larger J_{SC} and FF than solar cells with a C_{70} as the dedicated ETL (i.e., type III with C_{70} ETL instead c-TiO_2), as reported previously.[7] It is worth noting that the latter only reached PCEs larger than 10% when based on incontinuous C_{70} films.[7] Therefore, different photovoltaic behavior of the type I devices versus the cells with C_{70} ETL may be concluded. This finding was supported by the STEM characterization (Figure 2), which suggests that there is no C_{70}/perovskite planar heterojunction in the cross section of the glass/FTO/$MAPbI_3$:C_{70} samples.

To gain a further insight into the C_{70} effect in the solar cell performance, type I devices were prepared from $MAPbI_3$:C_{70} blend films processed from solutions with different C_{70} concentrations. Figure 3 shows the statistics of the different photovoltaic parameters as a function of the C_{70} to $PbCl_2$ ratio in the precursor solution. In general, an increasing trend as a function of C_{70} content was detected, especially for the V_{OC} and FF. The improvement may be correlated to the pinhole evolution of the perovskite films (Figure S4). Furthermore, taking into account the carbon accumulation detected in the Carbon K-edge EELS map (Figure 2b), C_{70} may also play other roles, such as defect passivation at the perovskite grain boundaries as previously suggested for other carbon nanostructures (e.g., PCBM[11,12]).

As a result, the best PCE was obtained for the devices prepared through C_{70}-saturated perovskite solutions (1:4320 C_{70}/$PbCl_2$ ratio), pointing out that higher concentration values of C_{70} lead to more efficient solar cells.

Co-solvent approach

Taking into account the increasing PCE trend with C_{70} content, solvents with the ability to dissolve larger amounts of C_{70} were considered as co-solvents. In particular, *o*-xylene was chosen, not only because of its superior C_{70}-solubilising ability (i.e., ~4 mg mL^{-1}), although significantly lower than previously reported,[16] but also its inert character with respect to the perovskite precursors. Several series of $MAPbI_3$:C_{70} blend films were deposited from *o*-xylene/DMF (1:4 *v*/*v*) solutions with different C_{70}/$PbCl_2$ ratios (i.e., from 1:10000 to saturation at 1:2170). The obtained films were used to prepare solar cells with type I architecture (Scheme 1). Interestingly, the best PCE conversion was reached for the 1:4320 C_{70}/$PbCl_2$ ratio, which is the saturation value for the perovskite solution in DMF. However, adding *o*-xylene resulted in a significant increase of the PCE, reaching 13.6% for the best devices (Figure 4 and Table 2).

Table 2. Photovoltaic parameters, under AM 1.5 G simulated sunlight, of the best semiconducting ETL-free solar cells based on $MAPbI_3$:C_{70} blend films processed from DMF/*o*-xylene (4:1) solutions with different C_{70}/$PbCl_2$ ratios.

C_{70}/$PbCl_2$	J_{SC} [mA cm^{-2}]	V_{OC} [mV]	FF [%]	PCE [%]
1:6000	15.7	1051	74.9	12.4
1:4320[a]	15.6	1054	75.2	12.4
1:4320	17.4	1059	74.1	13.6
1:2170	15.0	1065	76.5	12.2

[a] Solar cells processed from co-solvent-free solutions.

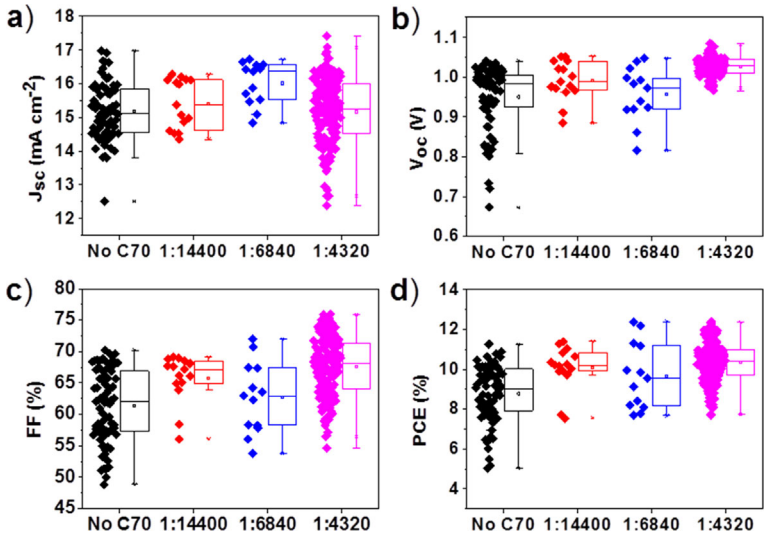

Figure 3. Statistics for the photovoltaic parameters a) V_{OC}, b) J_{SC}, c) FF, and d) PCE of the solar cells based on $MAPbI_3$:C_{70} blend films processed from formulations with different $C_{70}/PbCl_2$ ratios.

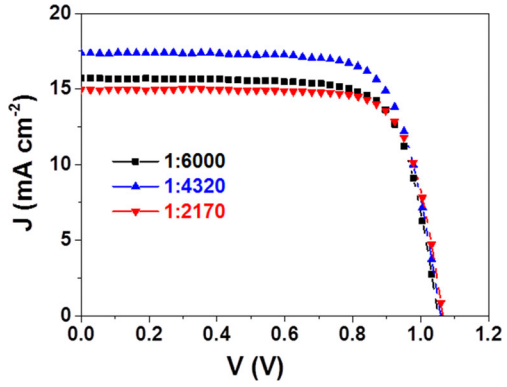

Figure 4. *J–V* characteristics, under AM 1.5 G simulated sunlight, of the best semiconducting ETL-free solar cells based on $MAPbI_3$:C_{70} blend films processed from different $C_{70}/PbCl_2$ ratios in DMF/*o*-xylene (4:1) solutions. The statistical analysis of the photovoltaic parameters can be found in Figure S5.

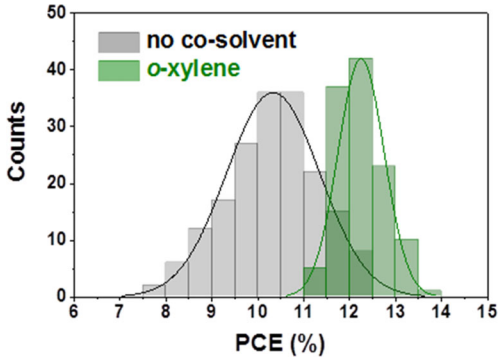

Figure 5. Statistical evaluation of the PCE of ETL-free solar cells based on $MAPbI_3$:C_{70} blend films processed with and without *o*-xylene (green and grey, respectively).

Indeed, the use of *o*-xylene resulted not only in a higher PCE, but also in considerably higher reproducibility (narrower dispersion, Figure 5) of the PCE values. This finding points out the enhanced robustness of the *o*-xylene co-solvent-based device preparation protocol.

Impedance spectroscopy

To gain further insight into the origin of the enhanced PCE of the ETL-free solar cells based on $MAPbI_3$:C_{70} blend films, devices with the different architectures (i.e., I, II, and III; Scheme 1) were analyzed under 1 sun illumination by impedance spectroscopy at different applied voltages. Figure 6a shows the representative Nyquist plot exhibiting two arcs and their fitting for each solar cell architecture. The fitting was carried out by using the previously reported equivalent circuit (Figure 6b).[17] The resistance of the high (R_3) and low (R_1) frequency arcs were related to injection and transport along the selective contacts[17,18] and to recombination, respectively.

Figure 6c shows a significant decrease of the R_3 resistance in ETL-free devices as could be expected owing to the absence of a semiconducting ETL and its consequent additional resistance contribution. However, for the $MAPbI_3$-based devices, there a large drop in the R_1 resistance was detected when the ETL-free architecture was used (Figure 6d), indicating an increase of the recombination rate. However, the decrease of R_1 was significantly damped when the $MAPbI_3$:C_{70} blend was used as the light harvesting film. Therefore, C_{70} seems to act as passivating agent for some perovskite defects and decreases thus the recombination loss pathways. It is noted that a similar effect was claimed for some fullerene derivatives, such as PCBM, in inverted architecture perovskite solar cells.[11]

Stability under AM 1.5 G simulated sunlight

The durability may be one of the main issues for the development of hybrid halide perovskite-based PVs. The effect of the

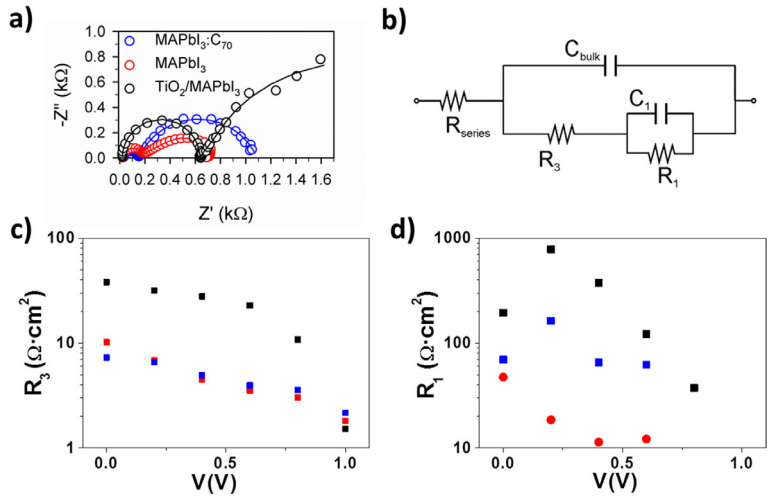

Figure 6. a) Nyquist plot of representative solar cells with different architectures under 1 sun illumination at 0 V applied bias, symbols correspond to the experimental points while solid lines correspond to the fitting of the impedance spectra using the b) equivalent circuit.[17] Resistances obtained from the impedance spectra fit: c) R_3, related to the transport and injection at selective contacts, and d) R_1, related to the recombination resistance.

$MAPbI_3$:C_{70} blend films on the photostability of unencapsulated perovskite solar cells was investigated. Figure 7 shows the evolution of the PV parameters versus time under continuous AM 1.5 G simulated sunlight for devices with architectures I, II, and III (Scheme 1). The *J–V* characteristics measured just before the photostability test (Figure S6), can be considered representative for such architectures.

It is worth to note that the solar cells based on $MAPbI_3$:C_{70} blend films (type I) exhibited the best V_{OC} and FF values after 10 min under illumination, reaching the same PCE that was estimated from the *J–V* characteristic measured under PCE maximization conditions (i.e., after applying a constant potential of 1.2 V, Figure S6 and Table S1). In contrast, the devices based on $MAPbI_3$ single films (type II and III) provided significantly lower V_{OC} and FF than those extracted from the *J–V* characteristics measured after applying constant potential. Furthermore, the solar cells based on $MAPbI_3$:C_{70} blend films (type I) showed enhanced photostability in comparison to architectures II and III. The J_{SC} and V_{OC} of type I devices suffered only about 10% reduction after 3 h under continuous illumination. Nevertheless, the FF decreased by approximately 25% of the initial value, which was the main cause of the 40% loss in the PCE. However, a PCE larger than 7% still remains after 3 h under 1 sun AM 1.5 G simulated sunlight, and no temperature control. Significant photostability improvement in comparison to the conventional regular architecture (i.e., III) can be highlighted. Although further investigations are needed to gain insights into origin of the photostability improvement, the significant en-

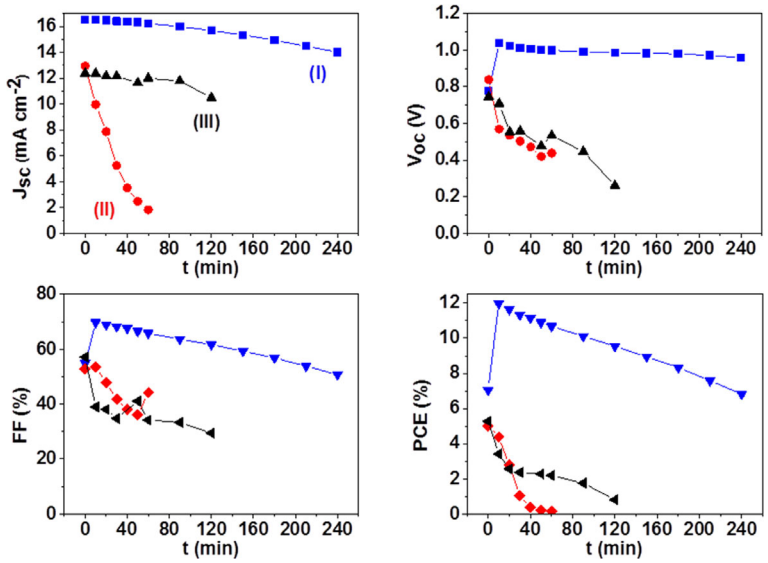

Figure 7. Evolution of the PV parameters versus time under continuous AM 1.5 G simulated sunlight for unencapsulated solar cells with different architectures (I: blue squares, II: red circles, and III: black triangles). a) J_{SC}, b) V_{OC}, c) FF, and d) PCE.

hancement detected in solar cells with regular architecture (i.e., including c-TiO_2 ETL) based on $MAPbI_3$:C_{70} blend films (Figure S7) provided a further support to claim the beneficial effect of the C_{70} addition. These findings, together with the recently reported photostability improvements reported for other carbon-based nanostructure additives, such as PCBM 1D nanorods,[13] seem to point towards some universality for carbon-based nano-additives and may open wide avenues for the development of stable perovskite solar cells.

Conclusions

A robust solution-processing protocol for the deposition of pinhole-free methylammonium lead triiodide ($MAPbI_3$)–C_{70}-fullerene blend films ($MAPbI_3$:C_{70}) on fluorine-doped tin oxide (FTO)-coated glass substrates and their integration into efficient (13.6% under AM 1.5 G simulated sunlight) semiconductor electron-transport layer (ETL)-free perovskite solar cells is demonstrated. The impedance spectroscopy analysis points out that ETL-free solar cells based on $MAPbI_3$:C_{70} exhibit larger recombination resistance (i.e., slower recombination rate) than those based on single $MAPbI_3$ films. This finding, together with lower transport resistance in comparison to the compact TiO_2 ETL-based devices, makes the glass/FTO/$MAPbI_3$:C_{70}/spiro-OMeTAD/Au a competitive heterostructure for perovskite solar cells. Furthermore, enhanced photostability of the unencapsulated $MAPbI_3$:C_{70}-based ETL-free solar cells is also demonstrated. The comparison of the photovoltaic performance versus the regular architecture perovskite solar cells based on C_{70} ETL[7] revealed significant differences, suggesting that other working principles than in planar junction solar cells are possible. The charge-transfer dynamic characterization of the $MAPbI_3$:C_{70} blend films is now in progress to gain further insight into the charge injection from the perovskite to the C_{70} and its influence on the solar cell performance. All in all, the present results open wide avenues for the deposition of perovskite–fullerene and/or derivatives blend films and their use in solar cells with simplified architecture, improved manufacturing process, and enhanced stability.

Experimental Section

Materials

The materials used in this study were obtained from commercial suppliers in high purity and used without further purification: glass/FTO (TEC15, Hartford Glass), C_{70} (99%, SES Research), MAI (DYESOL), $PbCl_2$ (98%, Sigma–Aldrich), spiro-OMeTAD (99%, Feiming Chemicals Limited), lithium bis(trifluoromethane) sulfonimidate (LiTFSI, 99.9%, Solvionic), *tert*-butylpyridine (96%, Sigma–Aldrich), DMF (extra pure, Scharlab), 2-propanol (synthetic grade, Scharlab), acetone (technical grade, Scharlab), chlorobenzene (99.8%, Sigma–Aldrich), toluene (99.8%, Sigma–Aldrich), *o*-xylene (98%, Sigma–Aldrich) and acetonitrile (UV HPLC grade, Scharlab).

Device fabrication

Glass/FTO samples were cleaned by the following procedure: the samples were sonicated in distilled water with soap for 5 min, rinsed thoroughly with distilled water, dried, and sonicated in acetone and 2-propanol for 15 min in each solvent.

The perovskite solution was prepared by dissolving 7.71 mmol of MAI and 2.57 mmol of $PbCl_2$ (molar ratio 3:1) in 3 mL of DMF and stirring overnight. Prior to deposition, the C_{70} was added to the perovskite solution. Different C_{70}/$PbCl_2$ ratios in the range from 1:14400 to 1:1270 were studied, as well as different co-solvents (i.e., *o*-xylene, toluene, and chlorobenzene) with the ratios 1:8, 1:4, and 1:2 (co-solvent/DMF). The resulting solution was spin coated on the substrates following a two-step protocol, which consisted of a first step of 500 rpm for 5 s followed by a second step of 2000 rpm for 45 s. Subsequently, the samples were annealed at 100 °C for 2 h to ensure complete perovskite formation.

On top of the perovskite layer, the spiro-OMeTAD hole-selective contact was deposited from a solution that contained spiro-OMeTAD (108.4 mg) in chlorobenzene (953.43 μL), LiTFSI solution in MeCN (17.17 μL, 520 mg μl^{-1}), and *tert*-butylpyridine (29.4 μL). The HTL was deposited by spin coating the solution at 3000 rpm for 30 s. The samples were left in a desiccator overnight. Finally, an array of round Au back contacts (~0.07 cm^2) was deposited by thermal evaporation at more than 5×10^{-6} torr with a NANO38 (Kurt J. Lesker) apparatus with a shadow mask.

Thin films and device characterization

The morphological properties of the films were analyzed with an ULTRA plus ZEISS FE-SEM. The chemical composition of the films was investigated by STEM. A Titan 60–300 (FEI, Netherlands) TEM equipped with EELS spectrometer (GIF Quantum 965, Gatan, U.S.A.) was used. The microscope was operated at 300 kV in STEM mode. EELS spectrum imaging (SI) in scanning mode gives access to spatially resolved EEL spectra. This method acquires a full resolution EELS spectrum at each pixel of the image. The recorded data cube is further processed to obtain spatial distribution of the signal arising from characteristic losses of particular atom species. The TEM lamellae were prepared by a standard FIB technique and polished by focused gallium beam to electron transparency (about 50 nm).

The *J*–*V* characteristics of the solar cells were measured under a xenon arc lamp simulator equipped with an AM 1.5 G spectral filter (Sun 2000, ABET Technologies). The intensity was adjusted to provide 1 sun illumination (100 mW cm^{-2}) by using a calibrated silicon solar cell. Unless otherwise mentioned, the *J*–*V* characteristics were recorded by scanning the potential from higher than the V_{OC} to zero (i.e., "reverse mode") at approximately 300 mV s^{-1}. Before the measurement, a voltage of approximately 1.2 V was applied to the devices for 1 min.

Stability measurements were carried out under continuous AM 1.5 G simulated sunlight, recording the *J*–*V* characteristics (in "reverse mode" and without applying any previous external voltage) every 10 min during the first 60 min, and from there every 30 min until PCE decreased at least 30% of its initial value.

The impedance spectroscopy measurements were performed under 1 sun illumination, AM 1.5 G (100 mW cm^{-2}) simulated sunlight (ABET Technologies, 1000 W Xe light source) previously calibrated with an NREL-calibrated Si solar cell. The measurements were carried out by means of a FRA equipped PGSTAT-30 from Au-

tolab at different forward voltage bias and applying a 20 mV voltage AC perturbation over the constant applied bias with the frequency ranging between 1 MHz and 0.05 Hz.

Acknowledgements

We thank Sandra Rodriguez for the excellent technical support. This work was partially supported by Basque Government and MINECO (Ministerio de Economía y Competitividad, Spain), under projects PC2015-1-03 (16-79), MAT2013-47192-C3-1-R MAT2013-47192-C3-2-R, CTQ2015-70921-P and MAT2015-70611-ERC. J.L.D. acknowledges Ikerbasque, the Basque Foundation for Science, for an "Ikerbasque Research Fellow" contract, Polymat Foundation, and MINECO of Spain for IEDI-2015-00666 grant. T.T.N. acknowledges the MINECO of Spain for her Ph.D. scholarship. J.P.M. and J.L.D. acknowledge Iberdrola Foundation for financial support.

Keywords: blend films · co-solvent · fullerene · perovskite · stability

[1] H.-S. Kim, C.-R. Lee, J.-H. Im, K.-B. Lee, T. Moehl, A. Marchioro, S.-J. Moon, R. Humphry-Baker, J.-H. Yum, J. E. Moser, M. Grätzel, N.-G. Park, *Sci. Rep.* **2012**, *2*, 591.

[2] M. M. Lee, J. Teuscher, T. Miyasaka, T. N. Murakami, H. J. Snaith, *Science* **2012**, *338*, 643 – 647.

[3] a) J. S. Manser, J. A. Christians, P. V. Kamat, *Chem. Rev.* **2016**, DOI: 10.1021/acs.chemrev.6b00136; b) S. F. Völker, S. Collavini, J. L. Delgado, *ChemSusChem* **2015**, *8*, 3012 – 3028; c) M.-H. Li, P.-S. Shen, K.-C. Wang, T.-F. Guoa, P. Chen, *J. Mater. Chem. A* **2015**, *3*, 9011 – 9019; d) S. Collavini, J. L. Delgado, *Adv. Energy Mater.* **2016**, 1601000.

[4] a) D. Liu, T. L. Kelly, *Nat. Photonics* **2014**, *8*, 133 – 138; b) J. You, L. Meng, T.-B. Song, T.-F. Guo, Y. Yang, W.-H. Chang, Z. Hong, H. Chen, H. Zhou, Q. Chen, Y. Liu, N. De Marco, Y. Yang, *Nat. Nanotechnol.* **2016**, *11*, 75 – 81.

[5] J. Song, E. Zheng, J. Bian, X.-F. Wang, W. Tian, Y. Sanehira, T. Miyasaka, *J. Mater. Chem. A* **2015**, *3*, 10837 – 10844.

[6] K. Wojciechowski, T. Leijtens, S. Siprova, C. Schlueter, M. T. Hörantner, J. T.-W. Wang, C.-Z. Li, A. K.-Y. Jen, T.-L. Lee, H. J. Snaith, *J. Phys. Chem. Lett.* **2015**, *6*, 2399 – 2405.

[7] S. Collavini, I. Kosta, S. F. Völker, G. Cabanero, H. J. Grande, R. Tena-Zaera, J. L. Delgado, *ChemSusChem* **2016**, *9*, 1263 – 1270.

[8] W. Ke, D. Zhao, C. R. Grice, A. J. Cimaroli, J. Ge, H. Tao, H. Lei, G. Fang, Y. Yan, *J. Mater. Chem. A* **2015**, *3*, 17971 – 17976.

[9] D. Liu, J. Yang, T. L. Kelly, *J. Am. Chem. Soc.* **2014**, *136*, 17116 – 17122.

[10] L. Huang, Z. Hu, J. Xu, X. Sun, Y. Du, J. Ni, H. Cai, J. Li, J. Zhang, *Sol. Energy Mater. Sol. Cells* **2016**, *149*, 1 – 8.

[11] Y. Shao, Z. Xiao, C. Bi, Y. Yuan, J. Huang, *Nat. Commun.* **2014**, *5*, 5784.

[12] J. Xu, A. Buin, A. H. Ip, W. Li, O. Voznyy, R. Comin, M. Yuan, S. Jeon, Z. Ning, J. J. McDowell, P. Kanjanaboos, J.-P. Sun, X. Lan, L. N. Quan, D. H. Kim, I. G. Hill, P. Maksymovych, E. H. Sargent, *Nat. Commun.* **2015**, *6*, 7081.

[13] C. Ran, Y. Chen, W. Gao, M. Wang, L. Dai, *J. Mater. Chem. A* **2016**, *4*, 8566 – 8572.

[14] L. Huang, J. Xu, X. Sun, Y. Y. Du, H. Cai, J. Ni, J. Li, Z. Hu, J. Zhang, *ACS Appl. Mater. Interfaces* **2016**, *8*, 9811 – 9820.

[15] W. Ke, G. Fang, J. Wan, H. Tao, Q. Liu, L. Xiong, P. Qin, J. Wang, H. Lei, G. Yang, M. Qin, X. Zhao, Y. Yan, *Nat. Commun.* **2015**, *6*, 6700.

[16] K. N. Semenov, N. A. Charykov, V. A. Keskinov, A. K. Piartman, A. A. B. Aleksei, A. Kopyrin, *J. Chem. Eng. Data* **2010**, *55*, 13 – 36.

[17] A. Guerrero, G. Garcia-Belmonte, I. Mora-Sero, J. Bisquert, Y. S. Kang, T. J. Jacobsson, J.-P. Correa-Baena, A. Hagfeldt, *J. Phys. Chem. C* **2016**, *120*, 8023 – 8032.

[18] E. J. Juarez-Perez, M. Wußler, F. Fabregat-Santiago, K. Lakus-Wollny, E. Mankel, T. Mayer, W. Jaegermann, I. Mora-Sero, *J. Phys. Chem. Lett.* **2014**, *5*, 680 – 685.

Received: July 14, 2016
Published online on ■■ ■■, 0000

J. Pascual, I. Kosta, T. Tuyen Ngo, A. Chuvilin, G. Cabanero, H. J. Grande, E. M. Barea, I. Mora-Seró, J. L. Delgado,* R. Tena-Zaera**

■■ – ■■

Electron Transport Layer-Free Solar Cells Based on Perovskite–Fullerene Blend Films with Enhanced Performance and Stability

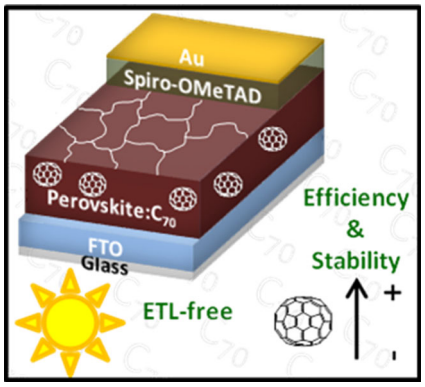

Mix, spin, go! Perovskite solar cells based on pinhole-free perovskite–C_{70} fullerene blend films deposited on fluorine-doped tin oxide (FTO)-coated glass substrates, without a specific electron-transporting/blocking layer, are fabricated and characterized. Enhanced photovoltaic performance and stability with respect to traditional compact TiO_2-based cells is achieved for these simplified devices under continuous AM 1.5 G simulated sunlight, without the need for encapsulation.